Hydrothermal Exploration of the southern Chile Rise: Sediment-hosted venting at the Chile Triple Junction.

Christopher R German[1], Tamara Baumberger[2], Marvin D. Lilley[3], John Edward Lupton[4], Abigail E. Noble[5], Mak A. Saito[6], Andrew Thurber[7], and Donna K Blackman[8]

[1]Wood Hole Oceanographic Institution
[2]Cooperative Institute for Marine Resources Studies, Oregon State University
[3]School of Oceanography, University of Washington
[4]NOAA-PMEL
[5]Woods Hole Oceanographic Institution
[6]WHOI
[7]College of Ocean Earth, Ocean & Atmospheric Sciences, Oregon State University
[8]University of California, Santa Cruz

November 22, 2022

Abstract

We report results from a hydrothermal plume survey along the southernmost Chile Rise from the Guamblin Fracture Zone to the Chile Triple Junction encompassing two segments (93km cumulative length) of intermediate spreading-rate mid-ocean ridge axis. Our approach used *in situ* water column sensing (CTD, optical clarity, redox disequilibrium) coupled with sampling for shipboard and shore based geochemical analyses (d^{3}He, CH_4, TDFe, TDMn) to explore for evidence of seafloor hydrothermal venting. Across the entire survey, the only location at which evidence for submarine venting was detected was at the southernmost limit to the survey. There, the source of a dispersing hydrothermal plume was located at 46°16.5'S, 75°47.9'W, coincident with the Chile Triple Junction itself. The plume exhibits anomalies in both d^{3}He and dissolved CH_4 but no enrichments in TDFe or TDMn beyond what can be attributed to resuspension of sediments covering the seafloor where the ridge intersects the Chile margin. From comparison with the Escanaba Trough on the southern Gorda Ridge, we infer that the anomalies we report here arise from sediment-hosted venting at the Chile Triple Junction.

Table S1: Water Column Analytical Data, RV Melville Cruise MV1003 (2010)

Location	Cast#	Bottle #	Latitude	Longitude	Depth (m)	∂3He (%)	CH4 (nM)	TDFe (nM)	TDMn (nM)
Seg 2	2T	1	45°41.4'S	76°52.1'W	4142	26.80	0.5		
Seg 2	2T	2			3999	28.66	0.6		
Seg 2	2T	3			3798	26.74	0.4		
Seg 2	2T	4	45°41.6'S	76°51.8'W	3596	26.79	0.5		
Seg 2	2T	5	45°45.5'S	76°47.8'W	3775		0.6		
Seg 2	2T	6			3600		0.6		
Seg 2	2T	7			3450		0.4		
Seg 2	2T	8	45°45.8'S	76°47.7'W	3300		0.3		
Seg 2	2T	9	45°49.9'S	76°46.6'W	3600	27.35	0.6		
Seg 2	2T	10			3425	27.25	0.6		
Seg 2	2T	11			3250	27.21	0.3		
Seg 2	2T	12			3075	28.29	0.7		
Seg 2	2T	13	45°50.4'S	76°46.6'W	2902	28.16	0.4		
Seg 2	2T	14	45°56.6'S	76°45.8'W	3705		1.1		
Seg 2	2T	15			3600		1.5		
Seg 2	2T	16			3500		1.1		
Seg 2	2T	17			3400		0.7		
Seg 2	2T	18	45°54.1'S	76°45.5'W	3250		0.8		
Seg 2	2T	19	45°57.0'S	76°40.3'W	3950	27.44	0.9		
Seg 2	2T	20			3795	27.47	0.5		
Seg 2	2T	21			3652	27.47	0.3		
Seg 2	2T	22			3500	27.68	0.3		
Seg 2	2T	23	45°57.3'S	76°39.8'W	3350	27.99	0.3		
A	1T	1	45°51.1'S	75°58.3'W	3228	24.42	2.1		
A	1T	2			3000	24.35	1.0		
A	1T	3			2750	26.56	1.0		
A	1T	4	45°51.2'S	75°58.2'W	2499	26.64	1.5		
B	1T	6	46°01.2'S	75°54.3'W	3200	26.48	0.9		
B	1T	7			2999	26.09	0.3		
B	1T	8			2750	28.44	0.4		
B	1T	9			2700	27.65	0.4		
B	1T	10	46°01.7'S	75°54.1'W	2500	27.94	2.0		
C	1T	11	46°08.3'S	75°51.9'W	3007	26.86	0.8		
C	1T	12			2900	27.56	0.6		
C	1T	13			2799	27.99	-0.2		
C	1T	14	46°08.5'S	75°51.7'W	2701	28.36	0.8		
D	1T	16	46°12.8'S	75°49.8'W	2899	28.09	4.7		
D	1T	17			2801	28.43	5.8		
D	1T	18			2700	31.00	18.1		
D	1T	19	46°13.0'S	75°49.6'W	2600	28.56	1.8		
E	1T	20	46°16.4'S	75°47.9'W	2600	34.58	26.3		
E	1T	21			2700	38.92	52.2		
E	1T	22			2800	33.80	26.9		
E	1T	23			2895	28.66	4.4		
E	1T	24	46°16.5'S	75°47.8'W	2500	30.82	7.7		
F	12V	9	46°15.4'S	75°48.4'W	2500	28.21	2.3	25.4	2.9
F	12V	6			2600	29.09	2.3	59.8	2.8
F	12V	5			2700	30.51	13.5	75.6	4.6
F	12V	4			2790	33.55	25.5	53.9	4.7
F	12V	3			2850	29.83	12.1	95.4	5.5
F	12V	2			2900	29.50	10.5	70.6	4.9
F	12V	1	46°15.4'S	75°48.4'W	2954	28.88	8.0	79.5	5.2

Hydrothermal Exploration of the southern Chile Rise: Sediment-hosted venting at the Chile Triple Junction.

C.R.German[1], T.Baumberger[2,3], M.D.Lilley[4], J.E.Lupton[3], A.E.Noble[1], M.Saito[1], A.R.Thurber[5] and D.K.Blackman[6]

[1]Woods Hole Oceanographic Institution, Woods Hole, MA 02543. [2] Pacific Marine Environmental Laboratory, National Oceanic and Atmospheric Administration, Newport,)R 97365. [3] Cooperative Institute for Marine Resources Studies, Oregon State University, Newport, OR 97365. [4] School of Oceanography, U.Washington, Seattle WA 98195. [5] College of Ocean Earth, Ocean & Atmospheric Sciences, Oregon State University, Corvallis, OR 97331. [6] Department of Earth & Planetary Sciences, UC Santa Cruz, CA 95064.

Corresponding author: Christopher German (cgerman@whoi.edu)

Key Points:

- Hydrothermal exploration along the southernmost Chile Rise has revealed evidence for venting located at the Chile Triple Junction.
- Hydrothermal plume signals include dissolved methane enrichments co-registered with diagnostic mantle-like Helium isotope signatures.
- Seafloor morphology, turbidity and TDFe, TDMn data all provide evidence that this is a sediment-hosted hydrothermal vent-field.

Abstract

We report results from a hydrothermal plume survey along the southernmost Chile Rise from the Guamblin Fracture Zone to the Chile Triple Junction encompassing two segments (93km cumulative length) of intermediate spreading-rate mid-ocean ridge axis. Our approach used *in situ* water column sensing (CTD, optical clarity, redox disequilibrium) coupled with sampling for shipboard and shore based geochemical analyses (δ^3He, CH_4, TDFe, TDMn) to explore for evidence of seafloor hydrothermal venting. Across the entire survey, the only location at which evidence for submarine venting was detected was at the southernmost limit to the survey. There, the source of a dispersing hydrothermal plume was located at 46°16.5’S, 75°47.9’W, coincident with the Chile Triple Junction itself. The plume exhibits anomalies in both δ^3He and dissolved CH_4 but no enrichments in TDFe or TDMn beyond what can be attributed to resuspension of sediments covering the seafloor where the ridge intersects the Chile margin. From comparison with the Escanaba Trough on the southern Gorda Ridge, we infer that the anomalies we report here arise from sediment-hosted venting at the Chile Triple Junction.

Plain Language Summary

Since their first discovery in the 1970s, submarine hot-springs have now been located in every ocean basin on Earth. But vast tracts (at least 75-80%) of the globe-encircling mid-ocean ridge volcanic chain remain completely unexplored which means that the majority of vents, and probably an increasing diversity of styles of submarine venting, remain to be discovered. The absence of discoveries is particularly acute in the southern hemisphere. Here we report results from the southern Chile Rise, close to the Chile Margin, where a segment of volcanic mid-ocean ridge crust is actively being subducted beneath the over-riding South American continental margin. The setting is unique in present-day tectonics, giving rise to unusual hydrothermal signatures. But the same processes may have recurred consistently around the rim of the Pacific throughout its ~200My history.

1 Introduction

Hydrothermal activity has been demonstrated to exist in all ocean basins and along ridges of all spreading rates [Baker & German, 2004] but the vast majority of mid-ocean ridges remain unexplored for seafloor venting; this is particularly the case in the southern hemisphere [Beaulieu et al., 2013]. Further, as exploration for seafloor venting has continued along different ridge-crests, the range in geologic diversity of known submarine hydrothermal fields has expanded [German & Seyfried, 2014; German et al., 2016]. The southern Chile Rise represents a particularly intriguing target from this perspective because, at its southernmost limit, it intersects the Peru-Chile Trench at the Chile Triple Junction (**Fig.1a**). This setting is geologically unique because it represents the only location on Earth at which a mid-ocean ridge is currently being subducted beneath a continental margin [Cande et al., 1987]. It is to be expected, however, that such processes have recurred throughout the ~200My history of the Pacific Ocean. Mapping of the southernmost four segments of the Chile Rise in 2010 provided new insights into the interplay among processes associated with crustal production at the Chile Rise ridge-crest and recycling of that ocean crust at the adjacent Peru-Chile Trench subduction zone [Blackman et al., 2012]. Here, we describe results from hydrothermal exploration conducted in conjunction with that mapping effort and in follow-up studies completed during a follow-on cruise in 2012. Although our geophysical investigations [Blackman et al., 2012] covered the four southernmost segments of the Chile Rise (numbered consecutively starting from the Chile Triple Junction), our hydrothermal investigations were restricted to the southernmost two second-order ridge-segments (**Fig.1b,c**).

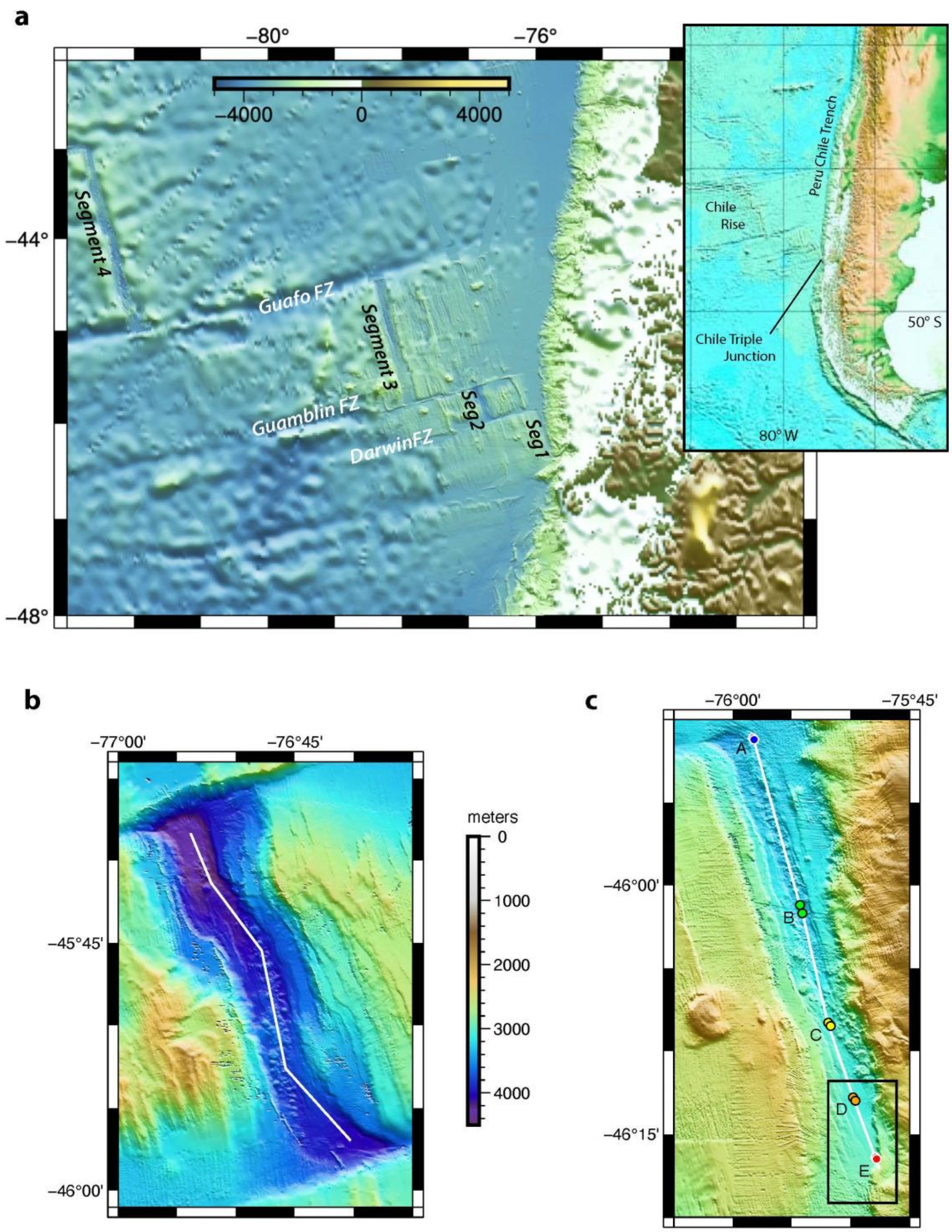

Figure 1. (a) *Inset:* regional map of the SE Pacific showing the location of the Chile Triple Junction in broad tectonic context. *Main figure*: map of the southernmost four segments of the Chile Rise mapped by Blackman et al. (2012); (b) detailed map of Segment 2 of the Chile Rise showing track-line of CTD tow-yo completed in 2010; (c) detailed map of Segment 1 of the Chile Rise showing trackline of CTD tow-yo completed in 2010, including (A-E) start/end locations for five mini-profiles of water column samples that were collected along-track. Box outlines region of 2012 field operations illustrated in Fig.3.

The Chile Rise is an intermediate spreading rate mid-ocean ridge with a half spreading rate of 30mm/yr which places it at a threshold in terms of underpinning geophysical processes that can impact morphology [Cande et al., 1987]. As a result of this spreading rate, variability in along-axis ridge morphology is apparent between segments [Blackman et al., 2012]. Segment 2, for example (Fig.1b) is anomalously deep for an intermediate spreading-rate ridge and exhibits a rift valley that is close to 1000 m deep relative to its flanks. Its axial depth is ~3800 m toward the center of this 43 km long segment and deepens to >4000 m at either end. In contrast, Segment 1 (Fig.1c), which is offset from Segment 2 by ~50 km along the Darwin Fracture Zone, is notably shallower with an axial rift-valley floor depth of ~ 3200 m at its northern end near 45°50’S. In prior work, the southern limit of Segment 1 and, hence, the location of the Chile Triple Junction (CTJ) had been estimated to occur at 46°09’S [Bourgois et al., 2000] where high back-scatter volcanic structures are juxtaposed against a scarp at the toe of the continental slope. With the higher resolution mapping conducted as part of our 2010 survey [Blackman et al., 2012], it was possible to identify fault scarps within the western rift-valley wall of Segment 1 that allow us to extend its length south to ~46°16’S (Fig.1c). The rift-valley floor reveals a chain of volcanic structures each <400 m in diameter that fall along the center-line of the graben at the northern end of the segment. Further south, beyond ~46°05’S, such features are increasingly obscured by terrigenous sediment shed from the adjacent continental margin. From 46°06’-46°12’S, some small volcanic features (diameter ~1 km each) are still discernible rising above the sediment fill [Blackman et al., 2012] but the morphology of the rift-valley floor becomes monotonously flat and featureless from ~46°12’ to the triple junction at ~46°16’S (Fig1c).

2 Materials and Methods

2.1 At Sea Operations & Sample Collection

The hydrothermal plume investigations described in this study were all conducted aboard RV Melville during two short cruises of opportunity conducted in 2010 (MV 1003) and 2012 (MV 1205). Surveys along the axis of the ridge-crest were first conducted using the ship’s Seabird 911+ CTD rosette which was equipped with a transmissometer and - specific to our work – two different *in situ* redox probes that were provided from NOAA-PMEL in 2010 and from AIST-Japan in 2012. Initially, the entire sensor suite was mounted to a 24-position rosette and towed at speeds of ~1.5 kt along the full length of each of Segment 2 and Segment 1 (Fig.1b, c) lowering and raising the package through the deep portion of the water column in “tow-yo” mode between depths of ~2500 m and a safe operating altitude above the seafloor (typically ~50m). Traditionally, such approaches have proven very effective at intercepting hydrothermal plumes dispersing away from high temperature hydrothermal fields [Baker & German, 2004] although it is now increasingly recognized that such approaches, in isolation, may under-report the full extent of submarine venting present along fast and intermediate spreading ridges [Baker et al., 2016; Chen et al., 2020]. In addition to these initial tow-yo surveys, vertical casts of the CTD-rosette package were conducted in 2010 while in 2012, a combination of tow-yo, vertical casts and "pogo" stations were employed. For the latter deployment type, the ship was repositioned over short distances to different locations to collect a series of vertical mini-profiles through the deep (>2500m) water column, within a single deployment. Importantly, an ultra-short baseline (USBL) navigation beacon was attached to the CTD-rosette for all deployments in 2010 and 2012 to ensure that we could navigate precisely where all samples and ancillary data were collected, as well as their sample depths (Suppl. Tables 1 & 2).

In parallel with our *in situ* sensing approach to hydrothermal plume detection, water samples were collected routinely. Initially, short mini-profiles (4-5 samples each) were collected at key way-points along the length of each of our segment-long "tow-yo" surveys, for a combination of shipboard and shore-based geochemical analyses diagnostic of submarine vent influence. First, from each Niskin, water samples were drawn for shore-based helium isotope analyses. Immediately upon recovery of the CTD-rosette, air-free water samples were flushed through 24 inch long sections of refrigeration-grade Cu tubing, with duplicate half-sections, and cold-weld sealed for on-shore laboratory determinations of He concentrations and isotope ratios [Young and Lupton, 1983]. Next, 100 mL of bubble-free fluid was drawn directly into 140 mL syringes for shipboard methane analysis. Any air bubbles were removed immediately after drawing the fluid into the syringe and this was followed by the addition of 40 mL headspace gas of ultrapure helium to the samples. The samples were then shaken vigorously and allowed to warm to room temperature (~ 30 min) to reach equilibrium for CH_4 between the water and gas phase, prior to shipboard analysis. In 2010, samples for total dissolvable Fe and Mn analyses were also archived into double-bagged 500mL polypropylene bottles that had been acid-washed for trace metal analyses prior to the cruise. Samples were drawn directly from the rosette into these sample bottles which were triple-rinsed with sample and then filled, unfiltered. Samples were transferred to Woods Hole Oceanographic Institution (WHOI) immediately upon completion of the cruise for trace-metal clean processing.

2.2 Laboratory Analyses of Samples

After the expedition, samples collected for Helium analyses were processed at the NOAA/PMEL Helium Isotope Laboratory in Newport, OR. The gas and liquid phases of the cold-welded samples were separated using a high-vacuum extraction line. The content of each sealed Cu tube was dropped into an evacuated flask and continuously stirred with a magnetic stirrer during the extraction process. A combined charcoal-LN_2 trap was then used to pump the gas phase into aluminosilicate ampoules during the 15 minute-long gas extraction process. The ampoules were subsequently sealed with a hot flame and stored dry until analysis. Isotope ratios and concentrations of helium were determined using a dual collector, 21 cm radius, sector-type mass spectrometer specially designed for helium isotope analyses. The precision for the helium isotope ratios in seawater samples averaged 0.2% in δ^3He, where δ^3He is the percentage deviation of $^3He/^4He$ from the atmospheric ratio.

Methane concentrations were determined at sea. After equilibration, the headspace gas was injected into a SRI 8610C gas chromatograph. Separation of CH_4 was done using a 15 m long Molecular Sieve 5A column and CH_4 concentrations were measured with a flame ionization detector. The measured background seawater CH_4 concentration was 0.4 nM. Sampling and analytical precision, determined through replicate draws, was <2.5% of the measured concentrations or ±0.1 nM, whichever is greater.

Analyses for total dissolvable iron (TDFe) and manganese (TDMn) were conducted on samples selected from Cruise MV1003 (2010) based on shipboard dissolved CH_4 data. Those analyses were conducted using Mg-precipitation, isotope dilution, and inductively coupled plasma mass spectrometry (ICP-MS) following standard methods described elsewhere [Saito and Schneider, 2006; Noble et al., 2008]. Briefly, unfiltered seawater samples were acidified to pH 1.7 using high purity HCl (SeaStar Inc) and then left for 4 months to allow the dissolution of labile metals in weak acid. For each analysis 13.0mL of processed sample was decanted into a centrifuge tube, spiked with ^{57}Fe stable isotope and precipitated using a small amount of high-purity ammonia (SeaStar Inc.) then centrifuged for 3 min at 3000 rpm (1460 x g) and decanted. The sample was resuspended in 5% high-purity nitric acid with 1ppm indium (In) and analysis was conducted on an Element 2 ICP-MS using an Aridus desolvator and platinum X-cones. Fe and Mn concentrations were calculated using the ^{57}Fe for isotope dilution and In as a recovery tracer [Saito and Schneider, 2006]. Precisions in the measurements were typically better than ±1.0nM for Fe and ±0.2nM for Mn.

3 Results & Discussion

3.1 Along-axis Surveys of the southern Chile Rise

Perhaps the most remarkable result from the initial tow-yo surveys conducted in 2010 (tow-yo tracks marked as white lines in Fig.1b, 1c) was that no *in situ* anomalies indicative of mid-water hydrothermal plumes were observed along the cumulative ~93km of survey. This was a surprise because prior work had shown that at least one site of high temperature hydrothermal venting should have been expected, statistically, during a survey of this length along an intermediate spreading-rate ridge [Baker & German, 2004; Beaulieu et al., 2013]. Further, shipboard and shore-based geochemical analyses for dissolved methane concentrations and He isotope composition also failed to detect hydrothermal signals throughout Segment 2 (*Supp.Table S1*).

Within Segment 1, by contrast, analyses for these dissolved gas species revealed clear evidence for seafloor hydrothermal inputs (**Fig.2**). Mini-profiles of water samples were collected at five locations along the length of this segment at 45°51'S, 46°01'S, 46°08'S, 46°13'S and 46°16'S (positions labelled A through E in Fig.1c, respectively). Throughout the northern half of the segment (locations A, B & C) no evidence for hydrothermal plume activity was apparent and values for both tracers fell into the same background range as was observed in Segment 2 (Supp. Table S1). This was the case at least as far as 46°08'S where sediment begins to obscure the underlying ridge-axis morphology [Blackman et al., 2012]. Further south, however, at locations D and E a clear mid-water plume is apparent in both the δ^3He anomaly profile and that for dissolved methane.

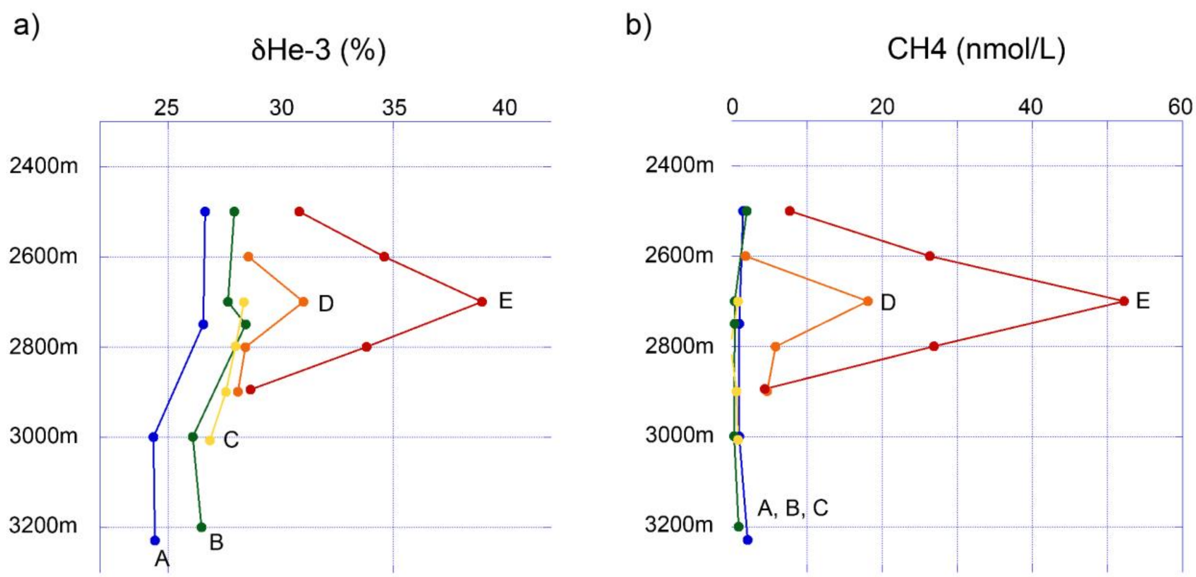

Figure 2. Vertical profiles of (a) δ^3He distributions and (b) dissolved CH_4 concentrations at each of locations A-E along the Segment 1 tow-yo trackline shown in Fig.1c.

In both cases, the maximum anomalies observed are at a depth of ~2700m with lower concentrations below and above that depth. Further, these anomalies occur at a height of ~200-300m above the seafloor at the southern end of Segment 1 consistent with the heights of rise that might be expected for a hydrothermal plume rising above a high-temperature vent-source before attaining a level of neutral buoyancy and being dispersed by prevailing deep ocean currents [Lupton, 1995]. For dissolved methane, the contrast between the background concentrations to the north of Segment 1 and the plume anomalies to the south are marked. Further, the range of concentrations observed (20-50nmol/L) is directly comparable to that observed for non-buoyant plumes overlying other high-temperature Pacific Ocean vent-sites [Lilley et al., 1995]. Along the Chile margin, immediately to the north of the Chile Triple Junction, thermal destabilization of gas hydrates beneath the sediments of the continental margin arises due to the increased heat-flow that results from subduction of young oceanic crust. This thermal destabilization leads to the accumulation of large amounts of gas hydrate in an extremely thin bottom-simulating reflector (BSR) layer at shallow depths within the sediment and can also lead to the release of dissolved methane via cold seep activity [Brown et al., 1996]. At the southern end of Segment 1, however, the presence of δ^3He anomalies that are unambiguously indicative of a mantle source [Lupton, 1983] coincident with the mid-water methane plume provides strong evidence that release of dissolved methane, here, is not due to cold seep activity. A high-temperature vent source is most consistent with the combination of mid-water mantle-signature δ^3He and dissolved CH_4 anomalies reported here.

3.2 Hydrothermal venting at the Chile Triple Junction.

We returned to the southern part of Segment 1 in 2012 to continue our exploration for this inferred hydrothermal source. Those operations began with a repeat tow-yo along the southern portion of the section occupied in 2010, between 46°16'S and 46°13'S (**Fig.3**) which, once again, revealed no *in situ* optical or redox anomalies indicative of hydrothermal venting but *did* exhibit mid-water plumes in δ^3He and dissolved CH_4. For both dissolved gas species, highest mid-water plume concentrations were observed at the southern end of the survey, closest to the intersection of the ridge-axis and margin (Supp. Table S2). Next, to confirm that the methane signals reported here were not related to cold-seep activity, a series of 4 vertical casts were occupied along the base of the scarp that defines the continental margin, immediately to the east of the ridge-crest (Area G). All samples from those mini-profiles yielded background values for both δ^3He (29.4±0.4%) and dissolved methane (4.4±1.4nmol/L) comparable to values from northern Segment 1 (Fig.4, Supp. Table S2).

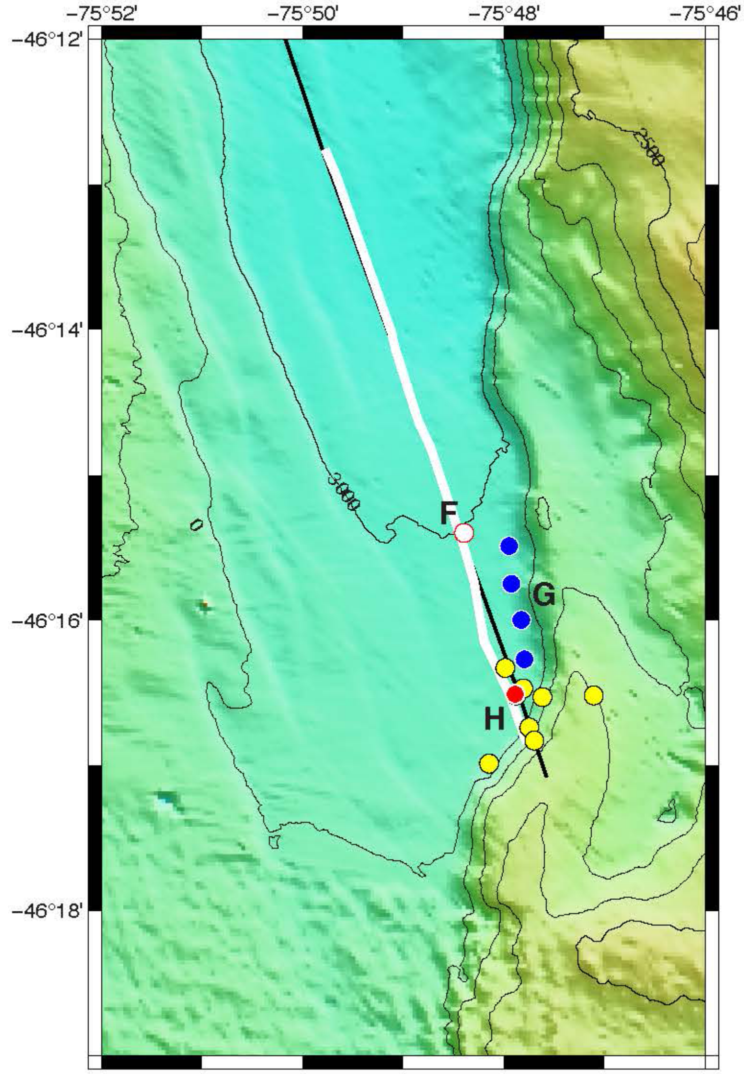

Figure 3. Map of the southernmost portion of Segment 1, southern Chile Rise (contour intervals: 100 m). White line denotes track of 2012 CTD tow-yo that reoccupied the southernmost portion of the 2010 tow-yo (underlying black line). Circles in areas F, G, H refer to vertical CTD profiles discussed in text. F (white): station sampled for δ^3He, CH_4, TDFe & TDMn in 2010; G (blue): stations along the Chile margin (2012); H (yellow, red): stations at the Chile Triple Junction (2012). Red circle represents point of closest approach to seafloor venting.

Three further sets of CTD-deployments were then undertaken, targeting the ridge-margin intersection at the CTJ (Area H). This yielded nine sets of vertical casts through the deep portion of the water column between 46°16'S and 46°17'S and between 75°46.5'W and 75°48.0'W (Supp. Tab. 2). All of these stations showed plume-height δ^3He anomalies that fell in the range 30-40%, compared to background values of 25-30% in northern segment 1, and dissolved CH_4 concentrations in the range 15-50nmol/L, clearly in excess over background (**Fig.4**). For both tracers, maximum anomalies were observed at ~2700m in a mini-profile that was occupied at 46°16.5'S, 75°47.9'W, collected quasi-synoptically with four other mini-profiles as part of a single CTD deployment. At this location, δ^3He and dissolved CH_4 values reached 38% and 46nmol/L respectively, marking the highest concentrations detected during our 2012 investigations and converging with our highest values from 2010 at the same location (Figs.2, 4).

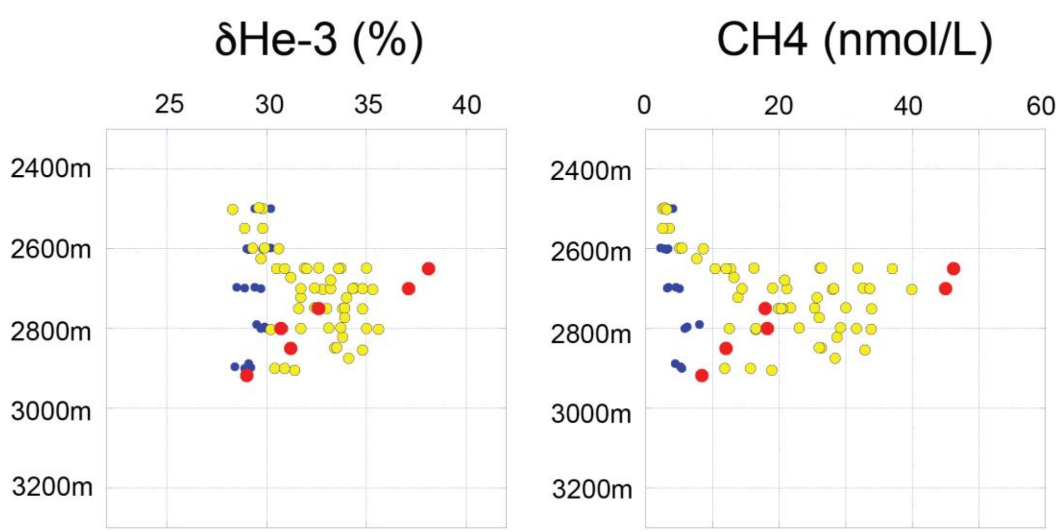

Figure 4. Vertical profiles of (*left*) δ^3He, and (*right*) dissolved CH_4 concentrations measured in southern Segment 1 in 2012. Color coding for symbols matches grouping of station locations shown in Fig.3. Blue = profiles from Chile margin with background values at all depths (Area G); Yellow, Red = profiles from Chile Triple Junction (Area H) that show hydrothermal anomalies in both δ^3He and CH_4 at plume depths; Red circles = profile with the highest plume anomalies.

From the much higher spatial resolution afforded from our 2012 surveys, we consider this location, as indicated by the red circle in Fig.3 (46°16.5'S, 75°47.9'W), to be our point of closest approach, thus far, to the source of seafloor venting at the Chile Triple Junction. Importantly, from an inter-comparison of δ^3He and dissolved CH_4 concentrations in all of our samples from southern Segment 1, we can be confident that there is only one such source. As shown in **Fig.5**, all of our hydrothermal plume data collected over both expeditions, from throughout the southern Segment 1 region (46°13-16'S) fall on a single linear trend that characterizes samples from both years. This can be taken as indicative that there is a single source of venting generating the plume signatures observed and, further, that this source was invariant over the timescale of repeat investigations of the region, consistent with a high-temperature vent-source located precisely at the Chile Triple Junction, where the southernmost Chile Rise ridge-axis is being subducted.

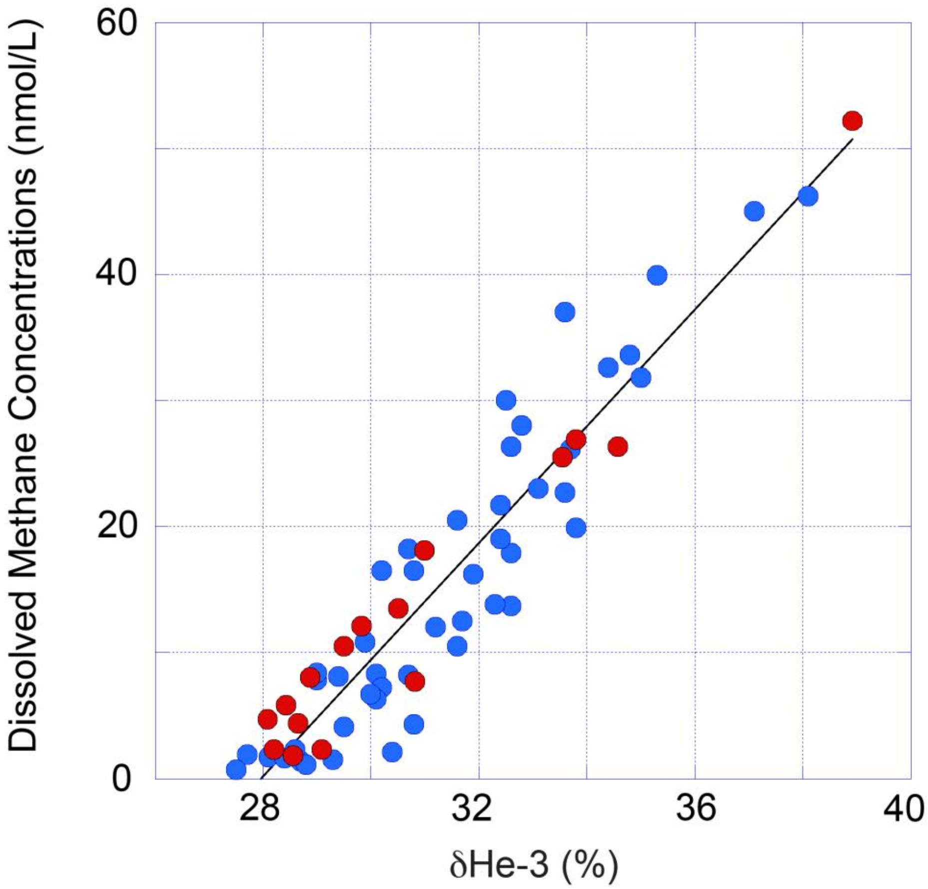

Figure 5. Plot of dissolved CH_4 concentrations vs δ^3He values for water-column stations at which hydrothermal plume anomalies were detected in both 2010 (Red Circles: Areas D, E, F) and 2012 (Blue Circles: Area H) all of which fall along a common linear trend (black line).

However, if the methane and δ^3He anomalies at the southern end of Segment 1 derive from a high-temperature hydrothermal source, a question that arises is why we could not detect the presence of ionic species arising from chemical (redox) equilibrium between the vent-fluids and the water-column using our *in situ* redox sensors that were mounted on the CTD-rosette. Remembering that all the hydrothermal plume signals from this study coincide with the southernmost portion of Segment 1, where sediment cover is sufficiently thick to obscure all volcano-tectonic morphologies [Blackman et al., 2012] provides a possible explanation for these observations. Examination of a cross-section of suspended particle concentrations, as determined from transmissometer data collected during the initial tow-yo survey in 2010 (**Fig.6a**), reveals that in addition to the seafloor being covered in thick sediment as the ridge-axis approaches the continental margin (Fig.1c), the overlying deep waters are characterized by a benthic nepheloid layer south of ~46°14'S that extends up to 2600m. These anomalies, which increase progressively toward the seafloor, are quite distinct from the particle-laden mid-water plumes that are typically observed overlying high-temperature "black smoker" vents.

The inference that there is extensive sediment resuspension in the deep waters of southern Segment 1 is supported by our analyses from a vertical CTD-station that was occupied toward the center of this region of Segment 1 in 2010 - station F (Fig.3). There, profiles for δ^3He and dissolved methane show diagnostic mid-water hydrothermal plumes (**Fig.6b**). Unlike those profiles, however, total dissolvable Fe and Mn data for the same samples show no coherent plume-like structure and, instead, exhibit a general increase toward the seafloor, reminiscent of the transmissometer cross-section (Fig.6a). Further, within the scatter of the data (which is far greater than the analytical precision of the measurements), there is even a suggestion that TDFe and TDMn concentrations exhibit a *decrease* at the depth at which highest δ^3He values and dissolved methane concentrations are observed. When interpreting these data, it is important to remember that TDFe and TDMn analyses were specifically adopted during early hydrothermal plume studies because this approach allows for the determination of both dissolved and recently-precipitated Fe and Mn concentrations in hydrothermal plumes at mid-ocean ridge settings where minimal terrigenous sediment is to be expected [Klinkhammer et al, 1985]. At the Chile Triple Junction, by contrast, sediment cover south of ~46°10'S is sufficient to mask any underlying volcano-tectonic morphology [Fig.1c; Blackman et al., 2012] and there is clear evidence for a thick benthic boundary layer that extends upward beyond the height of the non-buoyant hydrothermal plume height (Fig.6). This is important to consider because the level of acidification used during our sample processing was more than sufficient to redissolve authigenic FeMn-oxyhydroxide component of any sedimentary material incorporated into our samples [Bayon et al., 2002].

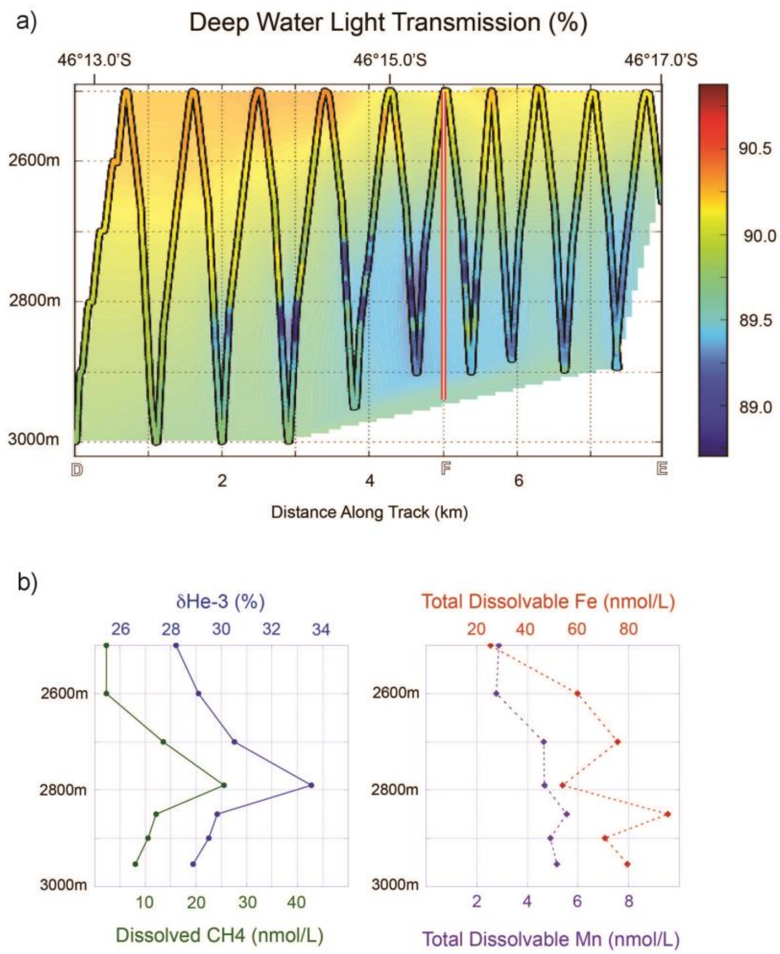

Figure 6. (a) Vertical cross-section of deepwater particle anomalies overlying the southern end of Segment 1 as detected from *in situ* transmissometer data collected during 2010 CTD tow-yo. Highest particle concentrations (lowest transmissometer values) are observed at the same latitudes where volcano-tectonic seafloor morphologies are obscured by sediment (Fig.1c, 2a). Vertical red bar shows location of CTD profile "F" (Fig.3); (b) vertical profiles from location "F" showing (left) δ^3He values & dissolved CH_4 with diagnostic mid-water hydothermal plumes and (right) TDFe & TDMn concentrations that, by contrast, increase progressively toward the seafloor.

3.3 Evidence for sediment-hosted venting at the Chile Triple Junction

A final consideration that arises concerning the TDFe and TDMn data reported here, is whether the absence of pronounced "black smoker" hydrothermal plume anomalies is because such signals are *masked* by the presence of inputs associated with sediment re-supension at the southern end of Segment 1, or whether such hydrothermally-sourced metal enrichments are altogether *absen*t. If the source of the δ^3He and dissolved methane concentrations observed at Station F was a typical "black smoker" vent, then we might predict plume-height CH_4:Mn ratios in the range 0.2-1.0, as reported previously from the northern East Pacific Rise [Baker et al., 1994]. In that case, for dissolved CH_4 anomalies of ~25nM (Fig.6b) we might expect corresponding TDMn anomalies of 25-125nM at hydrothermal plume height - *much* higher than the <10nM TDMn concentrations that we do observe. Instead, we argue that a more analogous setting to consider here is the Escanaba Trough at the southern limit of the Gorda Ridge [Atwater & Mudie, 1973]. Despite obvious differences in tectonic setting, what the Escanaba Trough shares in common with southernmost Segment 1 of the Chile Rise is that its axial rift-valley floor is also buried by terrigenous sediments, derived from the adjacent continental margin [Vallier et al., 1973]. In early water column studies at the Escanaba Trough, Baker et al. [1987] reported plume-like dissolved methane anomalies, at 200-300m above the seafloor, with no accompanying enrichments in Fe or Mn. While that study did not collect helium isotope samples to confirm the hydrothermal origins of the methane plume, subsequent Alvin dives located active vents at the NESCA hydrothermal field, discharging hot, clear fluids at temperatures up to 217±2°C [Campbell et al., 1994]. Those fluids were distinct from other mid-ocean ridge vents because they were (a) situated atop a thick sediment pile and (b) both cooler than, and highly depleted in transition metals compared to, typical "black smokers". Subsequent work showed that Fe and Mn are anomalously enriched in seafloor sediments at the same NESCA site, consistent with the sequestration of hydrothermally-sourced Fe and Mn that precipitate from the Escanaba vent-fluids into the sediments that the fluids percolate up through. Similar processes have also been documented at Middle Valley (Juan de Fuca Ridge) where ocean drilling has led to the characterization of extensive horizons of polymetallic sulfide within the subsurface at that ridge segment, which is also buried in terrigenous sediments [Zierenberg et al., 1998]. We hypothesize that the Chile Triple Junction hosts another example of the same style of venting; one in which high temperature vent-fluids circulating through young ocean crust at depth rise through the overlying sediment column, transporting their dissolved gas contents all the way to the seafloor but depositing their metal contents within the sediment column that they percolate up through. Upon reaching the seafloor, the emitted fluids – as at Escanaba Trough – remain sufficiently hot to form a buoyant hydrothermal plume that rises up above the seafloor until a level of neutral buoyancy is attained. This hypothesis would account for the generation of a plume that is enriched in ^{3}He and methane but devoid of high metal concentrations dispersing at mid-water depth away from a source of venting. In the case of the Chile Triple Junction our inference is that the source of this venting is located at the seafloor close to 46°16.5'S, 75°47.9'W.

4 Conclusions

We have conducted systematic exploration for evidence of hydrothermal venting along the southernmost two segments of the Chile Rise, from the Guamblin Fracture Zone to the Chile Triple Junction. Our results are consistent with a single source of high-temperature venting anywhere within this survey, at the southernmost end of Segment 1, immediately adjacent to where the mid ocean ridge-crest is being subducted, actively, beneath the Chile Margin. Hydrothermal plume signals in this vicinity are enriched in dissolved methane and helium isotope anomalies diagnostic of mantle influence in a mid-water lens consistent with a high-temperature vent-source at the underlying seafloor. But multi-beam bathymetry data for the same region provide evidence for thick terrigenous sediment sufficient to blanket neo-volcanic ridge axis morphologies. Further, optical back-scatter, TDFe and TDMn profiles overlying the sedimented southern-most portion of the ridge all show evidence for a benthic boundary layer, indicative of suspended sediment load, that extends upward from the seafloor to depths shallower than the hydrothermal plume layer. Importantly, however, the concentrations of TDFe and TDMn observed within this benthic boundary layer are too low to mask what would be expected in the non-buoyant plume of a conventional "black smoker" hydrothermal vent. Instead, we conclude that the most likely source of venting at the Chile Triple Junction is a sediment-hosted vent-site, emitting high-temperature fluids that are enriched in dissolved gases but depleted in dissolved metals. That vent-site, to within ≤1km, is predicted to be located at the seafloor close to 46°16.5'S, 75°47.9'W.

Acknowledgments

We thank our fellow scientists, the Captain and Crew of the RV Melville during cruises in 2010 and 2012 for their support in conducting the operations required to obtain the samples and data presented here. We also acknowledge the University of California who provided support for the shiptime that underpinned our research and the NOAA office of Ocean Exploration and Research who supported our research, both at sea and ashore.

Open Research

All data presented in this research are included in Supplementary Tables S1 and S2 appended to this submission.

References

Atwater, T. and Mudie, J.D. (1973), Detailed near-bottom geophysical study of the Gorda Rise. *J. Geophys. Res., 78*, 8665-8686.

Baker, E.T. and German, C.R. (2004), On the global distribution of mid-ocean ridge hydrothermal vent-fields. In "The Thermal Structure of the Oceanic Crust and the Dynamics of Seafloor Hydrothermal Circulation", *Geophys. Monogr. AGU, 148*, 245-266, 2004.

Baker, E.T., Massoth, G.J., Collier, R.W., Trefry, J.H., Kadko, D. Nelsen, T.A., Rona, P.A. and Lupton, J.E. (1987), Evidence for high-temperature hydrothermal venting on the Gorda Ridge, northeast Pacific Ocean. *Deep Sea Res., 34*, 1461-1476.

Baker, E.T., Feely, R.A., Mottl, M.J., Sansone, F.T., Wheat, C.G., Resing, J.A. & Lupton, J.E. (1994), Hydrothermal plumes along the East Pacific Rise, 8°40' to 11°50'N: plume distribution and relationship to apparent magmatic budget. *Earth Planet. Sci. Lett., 128*, 1-7.

Baker, E. T., Resing, J. A., Haymon, R. M., Tunnicliffe, V., Lavelle, J. W., Martinez, F., Ferrini, V., Walker, S. L., and Nakamura, K. (2016), How many vent fields? New estimates of vent field populations on ocean ridges from precise mapping of hydrothermal discharge locations. *Earth Planet. Sci. Lett., 449*, 186-196. doi: http://dx.doi.org/10.1016/j.epsl.2016.05.031

Bayon, G., German, C.R., Boella, R.M., Milton, J.A., Taylor, R.N. and Nesbitt, R.W. (2002), An improved method for extracting marine sediment fractions and its application to Sr and Nd isotopic analysis. *Chem. Geol., 187*, 179-199.

Beaulieu, S.E., Baker, E.T., German, C.R. and Maffei, A. (2013), An authoritative global database for active submarine hydrothermal vent fields. *Geochem. Geophys. Geosys., 14*, 4892–4905*.*

Beaulieu, S.E., Baker, E.T. & German, C.R. (2015), Where are the undiscovered hydrothermal vents on oceanic spreading ridges? *Deep Sea Res., 121*, 202-212*,* 2015.

Blackman, D.K., Applegate, B., German, C.R., Thurber, A.R. and Henig, A.S. (2012), Axial morphology along the Southern Chile Rise. *Mar. Geol*., *315*, 58-63.

Bourgois,J., Guivel, C., LaGabrielle, Y., Calmus, T., Boulegue, J. and Daux, V. (2000). Glacial-Interglacial trench supply variation, spreading ridge subduction, and feedback controls on the Andean margin development at the Chile Triple Junction area (45-48°S), *J. Geophys. Res*., *105*, 8355-8386.

Brown, K.M., Bangs, N.L., Froelich, P.N. and Kvenvolden, K.A. (1996), The nature, distribution and origin of gas hydrate in the Chie Triple Junction region. *Earth Planet. Sci. Lett*., *139*, 471-483.

Campbell, A.C., German, C.R., Palmer, M.R., Gamo, T. and Edmond, J.M. (1994), Chemistry of hydrothermal fluids from the Escanaba Trough, Gorda Ridge. In: "Geologic, Hydrothermal and Biologic Studies at Escanaba Trough" (Morton, J.L., Zierenberg, R.A. and Reiss, C.A., *eds*.), U.S.G.S. Bulletin *2022*, 201-221.

Cande, S.C., Leslie, R.B., Parra, J.C. and Hobart, M. (1987), Interaction between the Chile Ridge and Chile Trench: geophysical and geothermal evidence. *J. Geophys. Res*., *92*, 495-520.

Chen, S., Tao, C. and German, C.R. (2021), Abundance of low-temperature axial venting at the equatorial East Pacific Rise. *Deep Sea Res., 167,* doi.org/10.1016/j.dsr.2020.103426.

German, C.R. and Seyfried, W.E. Jr. (2014), Hydrothermal Processes. In: Holland H.D. and Turekian K.K. (eds.) Treatise on Geochemistry, Second Edition, Vol. 8, pp. 191-233, Oxford: Elsevier.

German, C.R., Barreiro, B.A., Higgs, N.C.. Nelsen, T.A., Ludford, E.M. and Palmer, M.R. (1995), Seawater metasomatism in hydrothermal sediments (Escanaba Trough, northeast Pacific). *Chem. Geol., 119*, 175-190, 1995.

German, C.R., Petersen, S. and Hannington, M. (2016), Hydrothermal exploration of Mid-Ocean Ridges: where might the largest sulfide deposits be forming? *Chem. Geol*., *420,* 114-126*.*

Klinkhammer, G., Rona, P., Greaves, M. and Elderfield, H. (1985). Hydrothermal manganese plumes in the Mid-Atlantic Ridge rift-valley. *Nature, 314*, 727-731.

Lilley, M.D., Feely, R.A., Trefry, J.H., (1995), Chemical and biological transformations in hydrothermal plumes. In: “Seafloor Hydrothermal Systems: Physical, Chemical, Biological, and Geological Interactions. *Geophys. Monogr. AGU, 91*, 369-391.

Lupton, J.E. (1995), Hydrothermal plumes: near and far field, in *Seafloor Hydrothermal Systems: Physical, Chemical, Biological, and Geological Interactions*. *Geophys. Monogr. AGU, 91*, 317-346.

Lupton, J.E. (1983), Terrestrial inert gases: isotope tracer studies and primordial components in the mantle. *Ann. Rev. Earth Planet. Sci., 11*, 371-414.

Noble, A.E., Saito, M.A., Maiti, K. and Benitez-Nelson, C.R. (2008), Cobalt, manganese, and iron near the Hawaiian Islands: A potential concentrating mechanism for cobalt within a cyclonic eddy and implications for the hybrid-type trace metals. *Deep Sea Res., 55,* 1473-1490.

Saito, M.A. and Schneider, D.L. (2006), Examination of precipitation chemistry and improvements in precision using the $Mg(OH)_2$ preconcentration inductively coupled plasma mass spectrometry (ICP-MS) method for high-throughput analysis of open-ocean Fe and Mn in seawater. *Anal. Chim. Acta*., *565*, 2, 222-233.

Vallier, T.L., Harold, P.J. and Girdley, W.A. (1973), Provenances and dispersal patterns of turbidite sand in Escanaba Trough, Northeastern Pacific Ocean. *Mar. Geol.*, *15*, 67-87.

Young, C. & Lupton, J.E. (1983), An ultratight fluid sampling system using cold-welded copper tubing. *EOS Trans. AGU*, *64*, 735.

Zierenberg, R.A., Fouquet, Y., Miller, D.J., Bahr, J.M.. Baker, P.A., Bjerkgard, T., Brunner, C.A., Duckworth, R.C., Gable, R., Gieskes, J., Goodfellow, W.D., Groschel-Becker, H.M., Guerin, G., Ishibashi, J., Iturrino, G.J., James, R.H., Lackschewitz, K.S., Marquez, L.L., Nehlig, P., Peter, J.M., Rigsby, C.A., Schultheiss, P., Shanks, W.C., Simoneit, B.R.T., Summit, M., Teagle, D.A.H., Urbat, M. & Zuffa, G.G. (1998), The deep structure of a sea-floor hydrothermal deposit. *Nature, 392*, 485-488.

Table S2: **Water Column Analytical Data, RV Melville Cruise MV1205 (2012)**

Location	Cast#	Bottle #	Latitude	Longitude	Depth (m)	∂3He (%)	CH4 (nM)
TowYo	1T	1	46°16.49'S	75°47.96'W	2866	29.4	8.1
TowYo	1T	2			2785	30.1	8.3
TowYo	1T	3			2689	33.6	22.7
TowYo	1T	4			2595	28.1	1.7
TowYo	1T	5	46°16.15'S	75°48.20'W	2500	28.7	1.4
TowYo	1T	6	46°15.74'S	75°48.30'W	2901	29.0	7.8
TowYo	1T	7			2797	32.6	13.7
TowYo	1T	8			2698	32.3	13.8
TowYo	1T	9			2602	27.7	1.9
TowYo	1T	10	46°15.50'S	75°48.40'W	2499	28.4	1.6
TowYo	1T	11	46°14.80'S	75°48.74'W	2901		1.6
TowYo	1T	12			2800	30.2	7.2
TowYo	1T	13			2700	30.7	8.2
TowYo	1T	14			2598	28.6	2.3
TowYo	1T	15	46°14.64'S	75°48.85'W	2502	27.5	0.7
TowYo	1T	16	46°14.14'S	75°49.08'W	2507	28.8	1.1
TowYo	1T	17			2602	29.3	1.5
TowYo	1T	18			2701	29.5	4.1
TowYo	1T	19			2800	31.6	10.5
TowYo	1T	20	46°14.02'S	75°49.12'W	2901	30.1	6.3
TowYo	1T	21	46°12.94'S	75°49.67'W	2800	30.0	6.7
TowYo	1T	22			2700	30.8	4.3
TowYo	1T	23			2602	29.9	10.8
TowYo	1T	24	46°12.76'S	75°49.78'W	2500	30.4	2.1
G	2P	1	46°15.49'S	75°47.95'W	2896	28.4	5.2
G	2P	2			2800	30.0	5.8
G	2P	3			2697	28.5	3.4
G	2P	4	46°15.49'S	75°47.95'W	2600	29.8	3.3
G	2P	5	46°15.75'S	75°47.93'W	2900	28.9	5.4
G	2P	6			2790	29.5	8.0
G	2P	7			2700	29.7	5.0

G	2P	8			2600	29.0	2.7
G	2P	9	46°15.75'S	75°47.93'W	2500	29.4	3.2
G	2P	10	46°16.00'S	75°47.83'W	2898	29.2	5.3
G	2P	11			2800	29.7	5.8
G	2P	12			2697	29.4	4.5
G	2P	13			2598	30.2	2.2
G	2P	14	46°16.00'S	75°47.83'W	2500	30.2	4.0
G	2P	15	46°16.27'S	75°47.80'W	2888	29.1	4.4
G	2P	16			2796	29.9	6.2
G	2P	17			2699	28.9	3.2
G	2P	18			2602	29.1	3.1
G	2P	19	46°16.27'S	75°47.80'W	2500	29.7	3.6
H	3P	1	46°16.33'S	75°47.99'W	2803	30.2	16.5
H	3P	2			2748	32.4	21.7
H	3P	3			2699	34.4	32.6
H	3P	4	46°16.33'S	75°47.99'W	2649	33.7	26.1
H	3P	5	46°16.52'S	75°47.11'W	2800	30.8	16.5
H	3P	6			2750	31.6	20.5
H	3P	7			2702	35.3	39.9
H	3P	8	46°16.52'S	75°47.11'W	2649	31.9	16.2
H	3P	9	46°16.51'S	75°47.89'W	2918	29.0	8.4
H	3P	10			2850	31.2	12.0
H	3P	11B			2800	30.7	18.2
H	3P	12			2750	32.6	17.9
H	3P	13			2700	37.1	45.0
H	3P	14	46°16.51'S	75°47.89'W	2650	38.1	46.2
H	3P	15	46°16.53'S	75°47.62'W	2800	31.7	12.5
H	3P	16			2750	33.8	19.9
H	3P	17			2702	32.8	28.0
H	3P	18	46°16.53'S	75°47.62'W	2650	33.6	37.0
H	3P	19	46°16.74'S	75°47.75'W	2799	33.1	23.0
H	3P	20			2748	32.5	30.0
H	3P	21			2699	32.4	19.0
H	3P	22	46°16.74'S	75°47.75'W	2648	32.6	26.3
H	3P	23	46°16.83'S	75°47.70'W	2700	34.8	33.6

H	3P	24	46°16.83'S	75°47.70'W	2649	35.0	31.8

H	4V	1	46°16.99'S	75°48.15'W	2905	31.4	18.9
H	4V	3			2875	34.1	28.4
H	4V	4			2854	34.8	32.9
H	4V	6			2802	35.6	33.8
H	4V	8			2751	34.8	33.9
H	4V	10			2700	34.3	28.2
H	4V	12			2650	32.0	12.7
H	4V	14			2600	30.6	8.6
H	4V	16			2549	29.8	3.5
H	4V	17	46°16.99'S	75°48.15'W	2500	29.8	2.5

H	5P	1	46°16.52'S	75°47.88'W	2900	30.4	11.8
H	5P	2			2849	33.4	26.3
H	5P	3			2800	35.0	31.6
H	5P	4			2749	33.9	25.3
H	5P	5			2723	34.0	25.7
H	5P	6			2700	33.2	21.1
H	5P	7			2679	33.2	20.8
H	5P	8			2650	30.5	12.0
H	5P	9			2625	29.7	7.6
H	5P	10			2599	29.3	5.0
H	5P	11			2549	28.9	2.5
H	5P	12	46°16.52'S	75°47.88'W	2498	29.6	2.8

H	5P	13	46°16.47'S	75°47.81'W	2900	30.9	15.7
H	5P	14			2848	33.5	26.0
H	5P	15			2822	33.8	28.7
H	5P	16			2798	33.7	29.2
H	5P	17			2773	33.9	26.0
H	5P	18			2750	33.0	20.3
H	5P	19			2722	31.7	13.8
H	5P	20			2700	31.7	14.4
H	5P	21			2672	31.2	13.2
H	5P	22			2650	30.9	10.4
H	5P	23			2598	29.9	5.4
H	5P	24	46°16.47'S	75°47.81'W	2502	28.3	3.1